Biomaterials Science

ROYAL SOCIETY OF CHEMISTRY

PAPER

View Article Online
View Journal | View Issue

Cite this: *Biomater. Sci.*, 2025, **13**, 3354

Development of MgO-loaded PLA/dECM antibacterial nanofibrous membranes for enhanced gingival regeneration†

Shu Sun,‡[a] Jing Qin,‡[b] Yifu Zhuang,‡[c] Pengfei Cai,[a] Xiao Yu,[a] Hongsheng Wang,[a] Xiumei Mo,[a] Jinglei Wu,[a] Mohamed EL-Newehy,[d] Meera Moydeen Abdulhameed,[d] Mingyue Fan,*[b] Wenhao Qian*[b] and Binbin Sun*[a]

Received 11th October 2024,
Accepted 26th April 2025

DOI: 10.1039/d4bm01346h

rsc.li/biomaterials-science

Clinically, gingival tissue repair is challenging due to the complex oral microbial environment and inflammation. The development of gingival membranes using tissue engineering techniques offers a promising solution to this issue. This study focuses on developing a nanofibrous gingival membrane, combining polylactic acid (PLA), decellularized extracellular matrix (dECM), and magnesium oxide (MgO) nanoparticles. Electrospinning was used to fabricate membranes with varying ratios of PLA, dECM, and MgO, and their mechanical, antibacterial, and cell-proliferation properties were evaluated. NIH-3T3 and rat gingival fibroblast (RGF) cells were cultured on the membranes to assess biocompatibility. A rat model with gingival defects was used to test *in vivo* tissue regeneration. It was indicated that the antibacterial nanofibrous membranes with MgO showed enhanced antibacterial effects and reduced inflammation, and promoted gingival tissue repair.

1 Introduction

Periodontal tissue is a highly stratified organ composed of embedded soft tissues (gingiva and periodontal ligament) and hard tissues (alveolar bone).[1] In fact, periodontal disease is an infection of periodontal tissues caused by bacteria, leading to inflammation accompanied by gingival recession. The accumulation of microbial biofilms (plaque) at the interface between the teeth and adjacent gingiva induces inflammation.[2] When inflammation penetrates deeper into the tissues, it results in extensive damage to both soft and hard tissues. Periodontitis can lead to severe destruction of the alveolar bone and gingival recession, eventually resulting in tooth loss.[3] Clinically, in severe cases of gingival recession, treatment usually requires mucogingival surgery, primarily through autologous soft tissue grafts.[4,5] However, this approach faces challenges such as limited donor tissue availability and the pain caused by secondary trauma to the patient.

In recent years, the advancement of tissue engineering technology has made it possible to construct tissue-engineered scaffolds *in vitro* and transplant them to sites of tissue defects, offering an ideal approach for tissue regeneration and repair. This is also of significant importance for the treatment of gingival defects.[6,7] Electrospinning, a common method for fabricating tissue-engineered scaffolds, produces nanofibers with nano- and microscale structures, offering a high surface area and a structure similar to the natural extracellular matrix (ECM).[8] This promotes cell proliferation and adhesion, as well as regulating cell differentiation. Furthermore, through appropriate design, electrospun nanofiber scaffolds can achieve biomimetic properties, spatial structure, gradual degradability, and functionality, thus better facilitating periodontal tissue repair.[9] Electrospun biodegradable scaffolds with synthetic polymers (such as polylactic acid, polycaprolactone, polyglycolic acid, *etc.*) have been widely used in tissue engineering.[10] Studies have shown that mixing natural polymers (such as hyaluronic acid, collagen, decellularized matrix, *etc.*) with synthetic polymers can enhance their physicochemical properties and bioactivity, making them more beneficial for periodontal

[a]*Shanghai Engineering Research Center of Nano-Biomaterials and Regenerative Medicine, College of Biological Science and Medical Engineering, Donghua University, Shanghai 201620, China. E-mail: binbin.sun@dhu.edu.cn*
[b]*Shanghai Xuhui District Dental Center, Shanghai 200032, China. E-mail: 13918158162@163.com, pingyanlaoto@163.com*
[c]*Orthopaedic Traumatology, Trauma Center, Shanghai General Hospital, School of Medicine, Shanghai Jiao Tong University, Shanghai 201620, China*
[d]*Department of Chemistry, College of Science, King Saud University, P.O. Box 2455, Riyadh 11451, Saudi Arabia*

†Electronic supplementary information (ESI) available. See DOI: https://doi.org/10.1039/d4bm01346h

‡These authors contributed equally to this work.

tissue repair.[11,12] Therefore, attempts were made in this study to mix a decellularized dermal extracellular matrix (dECM) with PLA and to use electrospinning to fabricate gingival nanofibrous membranes.

For gingival tissue repair, the unique fibrous connective tissue structure significantly limits the possibility of self-repair in clinical settings. The nanofibers produced through electrospinning can effectively mimic the fibrous connective tissue structure of natural gingival tissue, promoting the adhesion and proliferation of gingival fibroblasts.[13,14] However, due to the unique environment of the oral cavity, the use of tissue-engineered scaffolds for gingival tissue repair still faces challenges such as limited blood supply, severe microbial infection, and intense inflammatory reactions.[15,16] In fact, the oral environment is an "open" wound, constantly exposed to microbial challenges from the microbial biofilm present in the oral cavity.[17] Therefore, it is important to construct tissue engineered scaffolds with antimicrobial functions.

It was found that nano magnesium oxide (MgO) exhibits broad-spectrum antibacterial activity.[18] Compared to other antibacterial materials, magnesium oxide possesses excellent biocompatibility, safety, and long-term efficacy, making it suitable for various biomedical applications.[1] Adriana-Patricia *et al.* studied nano MgO and highlighted their antibacterial properties against a few microorganisms, confirming the inhibitory effect of nano MgO on representative oral bacterial strains.[19] This may be due to the high surface area and reactivity of the nanoparticles, which directly interact with the bacterial cell wall and membrane, leading to membrane rupture, increased permeability, and the leakage of cellular contents, resulting in bacterial death. Additionally, magnesium oxide may induce the generation of reactive oxygen species (ROS), or the formation of magnesium ions may promote an alkaline environment, further inducing bacterial death and exhibiting antibacterial effects. Moreover, nano magnesium oxide has anti-inflammatory properties, possibly due to its ability to inhibit the release of inflammatory factors by macrophages or its antioxidant properties, which reduce oxidative stress levels and alleviate inflammation. Numerous studies have demonstrated the antibacterial and anti-inflammatory effects of nano magnesium oxide, which are of significant importance for gingival tissue repair.[20] Therefore, this study proposes combining nano magnesium oxide with PLA and dECM to fabricate an antibacterial and anti-inflammatory gingival membrane that promotes gingival tissue regeneration and repair.

In this study, based on the aforementioned background, a nanofiber gingival membrane loaded with nano magnesium oxide was prepared using electrospinning. First, the optimal ratio of PLA and dECM and the optimal content of nano magnesium oxide were determined through physicochemical characterization *in vitro*. Subsequently, the effects of the prepared materials on the proliferation behavior of NIH-3T3 and gingival fibroblasts were verified through *in vitro* cell experiments. Finally, a rat gingival defect model was constructed to evaluate the *in vivo* effects on gingival tissue regeneration and further explore its possible mechanisms.

2 Materials and methods

2.1 Materials

Polylactic acid (PLA) was sourced from Jinan Daigang Biotechnology Co. Ltd (Jinan, China), while the dermal decellularized extracellular matrix (dECM) was extracted from porcine dermal tissues through enzymatic digestion and chemical treatment with surfactants, following a protocol from a previous study.[21,22] Hexafluoroisopropanol (HFIP) was obtained from Shanghai Darui Chemical Co. Ltd (Shanghai, China) and magnesium oxide nanoparticles were supplied by Shanghai Aladdin Co. Rat embryonic fibroblasts (NIH-3T3) were provided by the Cell Bank of the Chinese Academy of Sciences (Shanghai, China) and primary rat gingival fibroblasts (RGF) were purchased from Wuhan Pricella Biotechnology Co. Ltd (Wuhan, China). All reagents related to cell culture and characterization were purchased from Shanghai Hi-Tech Biotechnology Co. Ltd (Shanghai, China).

2.2 Preparation and characterization of dECM/PLA nanofibrous membranes

Nanofibrous membranes of PLA/dECM were fabricated using electrospinning technology. dECM and PLA were dissolved in HFIP and stirred overnight to achieve a homogeneous solution with a concentration of 8% (w/v). Electrospinning solutions were prepared with PLA to dECM ratios of 9 : 1, 8 : 2, 7 : 3, 6 : 4, and 5 : 5 (w/w). The electrospinning parameters were set as: a voltage of 12 kV, a flow rate of 3 mL h^{-1}, and a collection distance of 15 cm. The resulting nanofibrous membranes were stored in a vacuum desiccator for future use.

The surface morphology of the nanofibrous membranes was examined using scanning electron microscopy (SEM, Phenom XL). Prior to observation, gold coating was performed using a sputter coater (SC7620) at 5 mA for 60 seconds at an acceleration voltage of 10 kV. Image J software was used to measure the diameters of 100 nanofibers and analyze the diameter distribution histogram along with statistical analysis for each group. Additionally, the porosity of each group was measured and analyzed using Image J.

To further characterize the mechanical properties of the nanofibrous membranes, a universal testing machine (HY-940FS) was employed to assess their tensile Young's modulus. The tensile speed was set at 1 mm min^{-1} and the strain range for calculating Young's modulus was 0–5%. A comprehensive evaluation of morphology, porosity, and mechanical properties was conducted to determine the optimal PLA to dECM ratio for subsequent studies.

2.3 Preparation and characterization of MgO-loaded nanofibrous membranes

To fabricate nanofibrous membranes loaded with MgO, electrospinning solutions containing different concentrations of MgO (0, 0.25%, 0.5%, and 1.0%) were prepared by mixing MgO with PLA/dECM (5 : 5). Using the aforementioned electrospinning parameters, nanofibrous membranes were produced

and designated as Pd–MgO-0, Pd–MgO-0.25, Pd–MgO-0.5, and Pd–MgO-1.0.

SEM was employed to observe the surface morphology of the four types of membranes. Additionally, elemental analysis (C, N, O, and Mg) was performed using energy-dispersive X-ray spectroscopy (EDS, Quantax 400) to determine the Mg content, followed by statistical analysis. Fourier-transform infrared spectroscopy (FTIR, Nicolet 6700) was used to characterize the chemical composition of the membranes, with samples mixed with potassium bromide, ground, and pressed into pellets for scanning in the 4000–500 cm^{-1} range at a resolution of 4 cm^{-1}. The crystalline structure of the MgO-loaded membranes was analyzed using X-ray diffraction (XRD) with Cu/Kα radiation, 40 kV voltage, 300 mA current, a scan speed of 6° min^{-1}, and a 2θ scan range of 10–60°.

Mechanical tensile testing was conducted using a universal testing machine (HY-940FS) to obtain stress–strain curves and calculate the ultimate stress, elongation at break, and Young's modulus. It is worth noting that the Pd–MgO-1.0 group showed poor mechanical properties, with the scaffold being too brittle for tensile testing. Consequently, this group was deemed unsuitable for gingival tissue engineering scaffolds and excluded from further analysis.

To simulate the *in vitro* degradation behavior of MgO-loaded nanofibrous membranes, artificial saliva (pH = 6.8) was used. Briefly, samples with a diameter of 20 mm were dried and weighed (W_0), then placed in 5 mL of artificial saliva at 37 °C with gentle shaking. The solution was replaced every two days for the first week and once a week thereafter. Samples were retrieved on days 3, 7, 14, 21, and 28, rinsed with deionized water, freeze-dried, and weighed (W_t) to assess mass loss. The residual mass was calculated using the following formula:

$$\text{Residual mass}\ (\%) = \left(\frac{W_t}{W_0}\right) \times 100\%.$$

Nanofibrous membranes degraded for 7, 14, 21, and 28 days were observed using SEM to evaluate changes in their surface morphology. To study the sustained release behavior of magnesium ions, phosphate-buffered saline (PBS) was used as the release medium. Circular samples with a diameter of 14 mm were immersed in 5 mL of PBS and placed under shaking conditions at 37 °C. At 1, 2, 3, 7, 14, 21, 28, and 34 days, 2 mL of the release medium was collected and replaced with 2 mL of fresh PBS. The concentration of magnesium ions in the collected solutions was measured using inductively coupled plasma atomic emission spectroscopy (ICP-AES, Prodigy) and cumulative release curves were generated for each group.

2.4 *In vitro* test of NIH-3T3 and RGF cells on MgO-loaded nanofibrous membranes

Nanofibrous membranes loaded with MgO (Pd–MgO-0, Pd–MgO-0.25, and Pd–MgO-0.5) were cut into 14 mm circular samples and placed into 24-well cell culture plates. The samples were sterilized with UV irradiation for 60 minutes, followed by immersion in 75% ethanol for 2 hours. After sterilization, the membranes were rinsed three times with sterile PBS. Prior to cell seeding, NIH-3T3 fibroblasts and RGF cells were expanded in a controlled culture environment (37 °C, 5% CO_2, and 100% humidity) using high-glucose DMEM supplemented with 10% fetal bovine serum (FBS) and 1% penicillin/streptomycin antibiotic cocktail. The cells were maintained through regular passaging at 80–90% confluence to ensure optimal viability, with complete medium replacement performed every 48 hours. For experimental consistency, only cells between passages 3 and 5 were used in subsequent experiments. Then, the cells were seeded onto the membranes at a density of 1×10^4 cells per well. The tissue culture plate (TCP) served as the control group, with at least three replicates for each group.

The NIH-3T3 cells were characterized by CCK-8 assays on days 1, 3, and 5, while the RGF cells were characterized on days 1, 2, and 5. The quantitative results of CCK-8 assays were statistically analyzed to assess the cytotoxicity and biocompatibility of the nanofibrous membranes across different groups. Additionally, live/dead staining (AM/PI) was performed on both cell types after a defined culture period to evaluate the cell spreading behavior of the materials.

For the NIH-3T3 cells cultured for 5 days, the samples were sequentially dehydrated using an ethanol gradient (30%, 50%, 70%, 90%, 95%, and 100%), with each dehydration step lasting 15 minutes. The samples were then transferred to a freeze-dryer for drying, followed by SEM observation to assess cell morphology and adhesion behavior on the fibrous surfaces. In addition, the scratch healing effect was photographed and obtained by establishing a scratch after seeding NIH-3T3 on the material and incubating it for 12 hours.

2.5 Antibacterial access of MgO-loaded nanofibrous membranes

To evaluate the antibacterial effect of magnesium oxide-loaded nanofibrous membranes, an absorbance-based method was used to measure their bacteriostatic rate. Briefly, sterilized nanofibrous membranes were inoculated with *Staphylococcus aureus* (*S. aureus*) and *Escherichia coli* (*E. coli*) at a concentration of 1×10^5 CFU mL^{-1}. The samples were incubated at 37 °C for 24 hours.

After incubation, the bacterial suspension from the membrane surface was serially diluted to 10 000-fold. The diluted suspensions were then spread on LB agar plates. Phosphate-buffered saline (PBS) was used in the same manner as a control. After incubating at 37 °C for another 24 hours, photographs were taken and the number of bacterial colonies in each group was recorded to calculate the bacteriostatic rate.

2.6 Animal evaluation

Twenty SD rats (male and female, 8–10 weeks old) were randomly divided into four groups (Control, Commercial, Pd–MgO-0, and Pd–MgO-0.25), with five rats per group. The rats were anesthetized with Zeletil 50 (50 mg kg^{-1}) *via* intraperitoneal injection. A full-thickness palatal incision measuring 2.0×0.5 mm^2 was created at the midpoint of the maxillary molar gingival margin in each rat. The three groups received appropriately shaped scaffolds implanted at the defect site, while one group served as a blank control with no material used. All animals had *ad libitum* access

to water and food post-surgery. The wound healing was monitored daily and the rats were euthanized on day 10. The defect sites and surrounding tissues were carefully exercised for further embedding and sectioning.

Post-operative tissue samples were subjected to histological and immunohistochemical staining to assess gingival tissue repair. Specifically, H&E staining and Masson's trichrome staining were performed to statistically analyze the thickness of the gingival epithelium and evaluate tissue proliferation. Immunohistochemical evaluation was conducted for COL-1 and VEGF to assess collagen formation and angiogenesis, and for TNF-α and IL-6 to evaluate inflammation. Additionally, quantitative analysis of positive areas from four immunohistochemical results was performed to assess tissue repair outcomes. All animal procedures were performed in accordance with the Guidelines for Care and Use of Laboratory Animals of Donghua University and approved by the Animal Ethics Committee of Donghua University.

2.7 Statistical analysis

Quantitative data from the experiments are presented as the mean ± standard deviation. Statistical analysis was performed using one-tailed tests and one-way analysis of variance (ANOVA). A p-value of less than 0.05 ($P < 0.05$) was considered statistically significant, indicated as $P < 0.05$. Each experimental group was tested with at least three parallel samples.

3 Results and discussion

3.1 MgO-loaded nanofibrous membrane preparation and physicochemical property characterization

A synthetic polymer of PLA and a natural polymer of dECM were chosen to fabricate gingival nanofibrous membranes. To identify the optimal material ratio, five types of nanofiber membranes were electrospun from varying PLA/dECM ratios (5 : 5, 6 : 4, 7 : 3, 8 : 2, and 9 : 1). SEM analysis revealed smooth

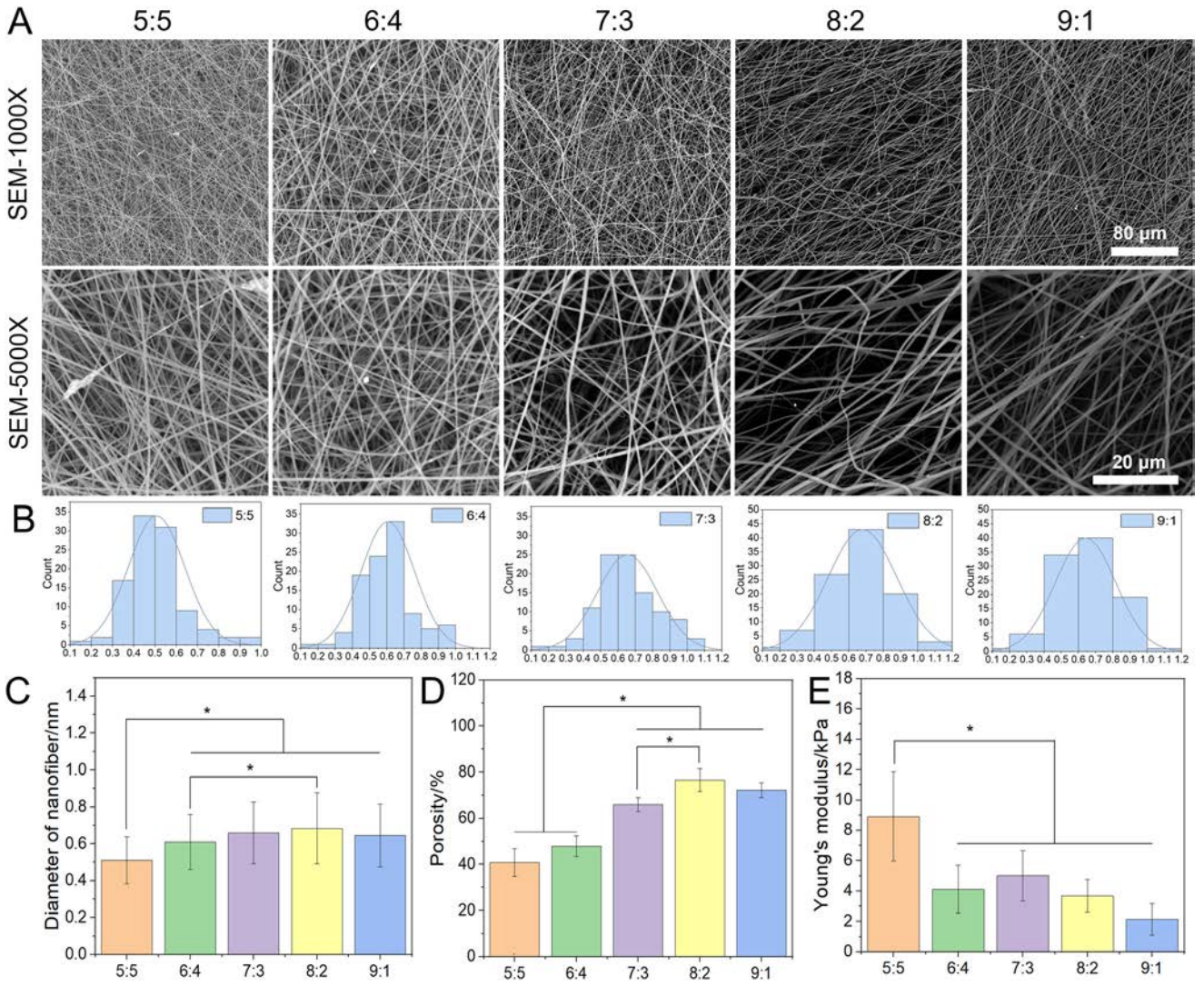

Fig. 1 SEM images (A) and diameter distribution histograms (B) of nanofiber membranes with different ratios. Statistical analysis of nanofiber diameter (C), porosity (D), and Young's modulus (E) at various ratios of nanofiber membranes.

nanofiber structures with uniform diameter across all groups (Fig. 1A and B). Diameter measurements indicated an increasing trend with higher PLA content, peaking at 8 : 2 (Fig. 1C), likely due to the increased viscosity of the spinning solution affecting the diameter of the nanofiber.[23] Fig. 1D shows that porosity also increased with the PLA content, possibly due to sparser fiber arrangement. Although the 5 : 5 ratio of the nanofibrous membrane exhibited the smallest fiber diameter and porosity, it demonstrated the highest Young's modulus, which might be due to the inherent brittleness of dECM.[24] Considering that mechanical properties are crucial for practical applications and that higher dECM content improves biocompatibility, the 5 : 5 ratio of PLA to dECM was selected for further investigation.

To incorporate nanomagnesium oxide (MgO), varying ratios of 0.25, 0.5, and 1.0 wt% MgO were blended with PLA/dECM (5 : 5). These mixtures were used to fabricate gingival nanofibrous membranes *via* electrospinning, labeled as Pd–

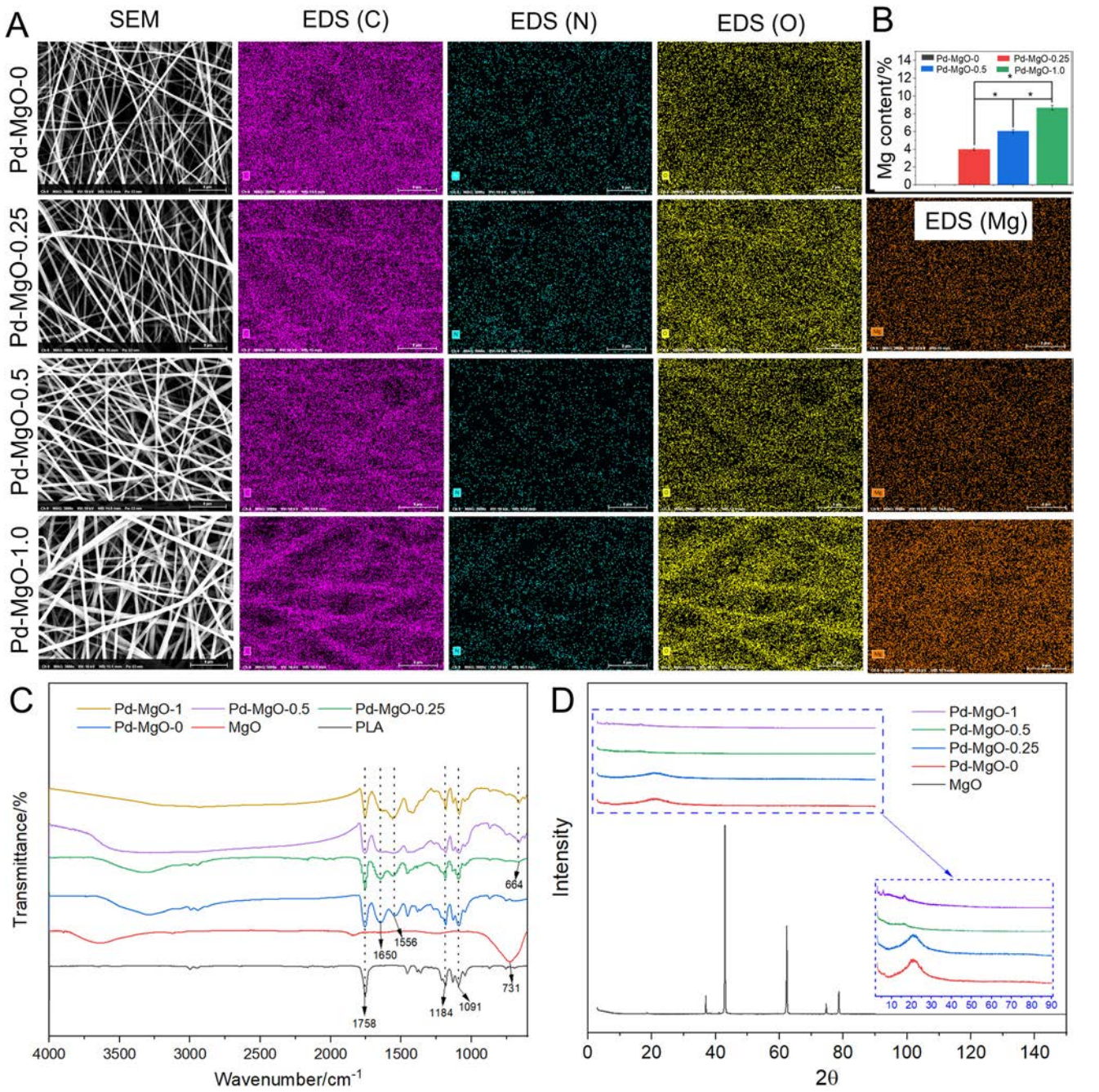

Fig. 2 SEM images and EDS mapping results (A) of nanofiber membranes loaded with different contents of MgO. Statistical analysis of Mg element content (B), and FTIR (C) and XRD (D) results of the nanofiber membranes loaded with different contents of MgO.

MgO-0.25, Pd–MgO-0.5, and Pd–MgO-1.0. The control membrane without MgO, referred to as Pd–MgO-0, was prepared similarly. SEM and EDS characterization indicated good fiber morphology and a proportional increase in Mg content with loading (Fig. 2A and B).

FTIR was performed to analyze the functional groups in different nanofiber membranes and PLA and MgO raw materials (Fig. 2C). The results indicated characteristic absorption peaks in PLA, such as the stretching vibration of the C=O bond at 1758 cm^{-1} and strong C–O stretching vibrations at 1184 cm^{-1} and 1091 cm^{-1}, confirming PLA's polyester properties.[25,26] These characteristic peaks were observed in all four nanofiber membrane groups, confirming the presence of PLA. The stretching vibration absorption peak of the Mg–O bond at 731 cm^{-1} was indicative of magnesium oxide, which appeared at 664 cm^{-1} in Pd–MgO-0.25, Pd–MgO-0.5, and Pd–MgO-1.0, but not in Pd–MgO-0, suggesting a shift in the absorption peak of the Mg–O bond.[27] This confirmed the successful loading of MgO. Notably, the presence of absorption peaks at 1650 cm^{-1} and 1556 cm^{-1} in all four nanofiber membrane groups indicated the presence of natural amide bonds in dECM.[28] Based on the XRD results in Fig. 2D, a characteristic Bragg reflection peak of magnesium oxide was observed at a scattering angle of 42°. However, all nanofibrous membranes displayed an amorphous morphology, consistent with previous findings that the nanofibrous membranes produced through polymer electrostatic spinning tend to be amorphous. Importantly, the characteristic peaks were not observed at the expected positions even when the nanofiber membranes were loaded with magnesium oxide. This could be attributed to the low content of magnesium oxide in the membrane.

Mechanical characterization of the three MgO-loaded nanofibrous membranes revealed increased brittleness at high MgO content (Pd–MgO-1.0), leading to inadequate mechanical integrity; thus, only the remaining materials were subjected to tensile testing (Fig. 3A). Statistical analysis of ultimate stress, elongation at break, and Young's modulus indicated that Pd–MgO-0.5 exhibited the highest stress and modulus, indicating that MgO enhances mechanical properties, although excessive content may impair toughness, leading to fragmentation

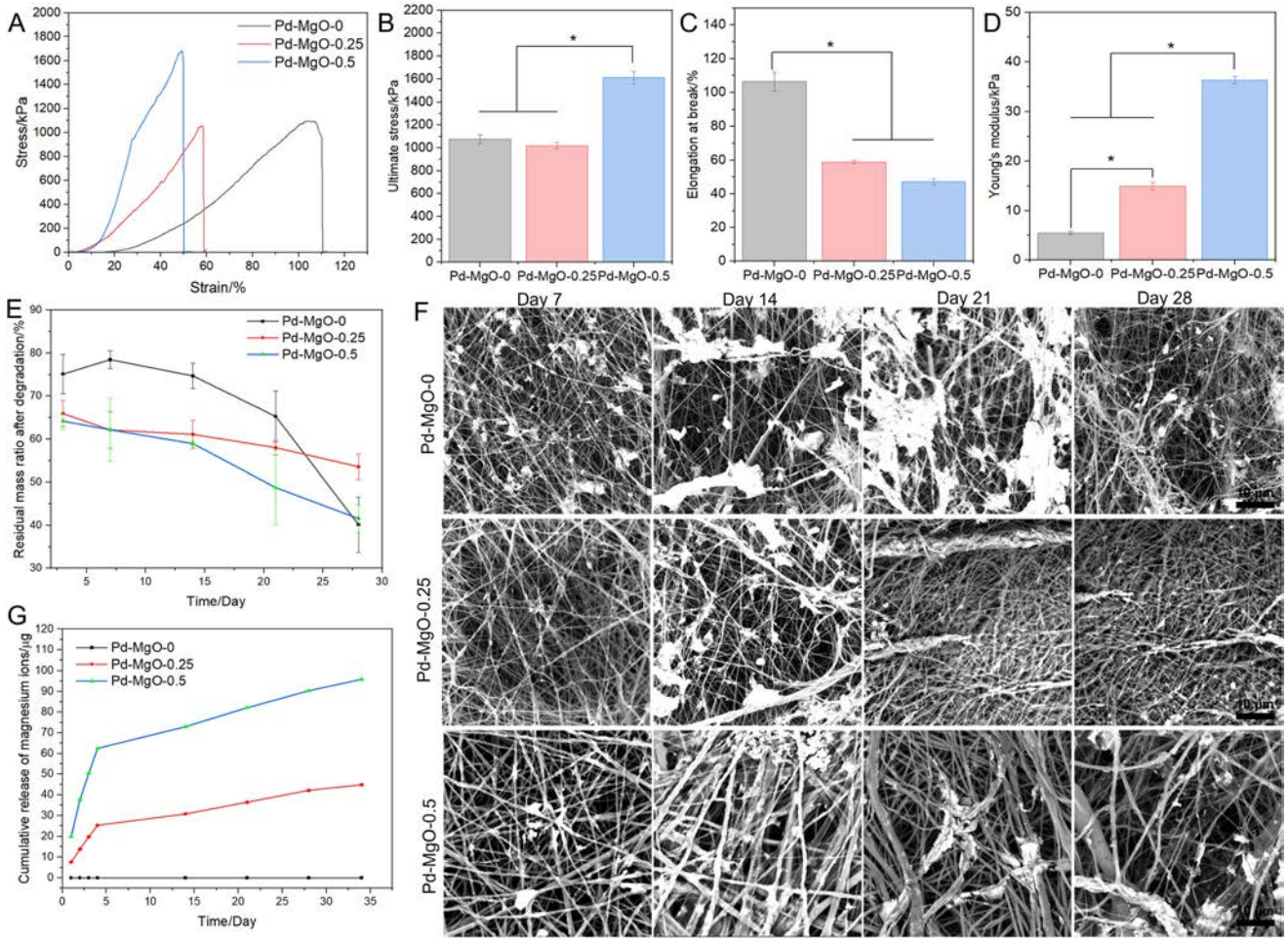

Fig. 3 (A) Stress–strain curves, (B) ultimate stress, (C) elongation at break, and (D) Young's modulus for various nanofibrous gingival membranes. (E) Residual mass percentage after degradation, (F) SEM morphology and (G) magnesium ion slow release curve of different nanofibrous gingival membranes.

(Fig. 3B–D). *In vitro* degradation tests showed morphological changes over time, with Pd–MgO-0 exhibiting significant fiber breakage, while Pd–MgO-0.25 and Pd–MgO-0.5 showed minimal alterations, suggesting that MgO addition slows degradation rates, consistent with degradation curves (Fig. 3E and F). ICP-MS quantified the sustained release of magnesium ions, showing significant release in the first five days, followed by a slower rate, with Pd–MgO-0.5 demonstrating double the cumulative release of Pd–MgO-0.25, aligning with theoretical expectations (Fig. 3G). The slow release of magnesium ions is significant for promoting angiogenesis and antibacterial effects, facilitating tissue regeneration and repair.[29] Studies by Qin *et al.* indicated that Mg ions activate the Notch signaling pathway, upregulating downstream genes Hes1 and Hes5 and angiogenesis-related genes HIF-1α and eNOS, promoting endothelial differentiation and enhancing stem cell migration and chemotaxis, which is crucial for tissue regeneration.[30]

3.2 Biocompatibility and antibacterial properties of MgO-loaded nanofibrous membranes

To evaluate the feasibility of nanofibrous gingival membranes for tissue engineering, we conducted *in vitro* studies by seeding NIH-3T3 and RGF cells on their surfaces. NIH-3T3, a common fibroblast cell line, is often used to assess material toxicity and biocompatibility.[31] After five days of culture, live/dead staining and CCK-8 assays indicated that Pd–MgO-0.25 exhibited the best biocompatibility, even promoting greater cell proliferation than TCP after culturing for 5 days (Fig. 4A and B). The SEM results showed better cell spreading on Pd–MgO-0.25 compared to other groups (Fig. 4C), indicating that MgO enhances biocompatibility, potentially through the sustained release of Mg ions promoting cell migration. However, high MgO content (Pd–MgO-0.5) showed cytotoxicity due to excessive Mg ion release. The enhanced cellular migration capacity was quantitatively confirmed through scratch wound healing assays. As demonstrated in Fig. S1,† nanofiber groups containing 0.25% and 0.5% MgO exhibited significantly improved wound closure rates compared to both MgO-free nanofibers and TCP control.

Furthermore, RGF cells, key in gingival repair, were extracted and cultured on membrane surfaces to assess oral gingival repair feasibility. Results (Fig. 5A and B) showed RGF cell proliferation trends similar to those for NIH-3T3, with Pd–MgO-0.25 demonstrating the highest proliferation effectiveness. Notably, cell proliferation on all gingival membranes was inferior to that for the TCP, indicating a preference for stiffer

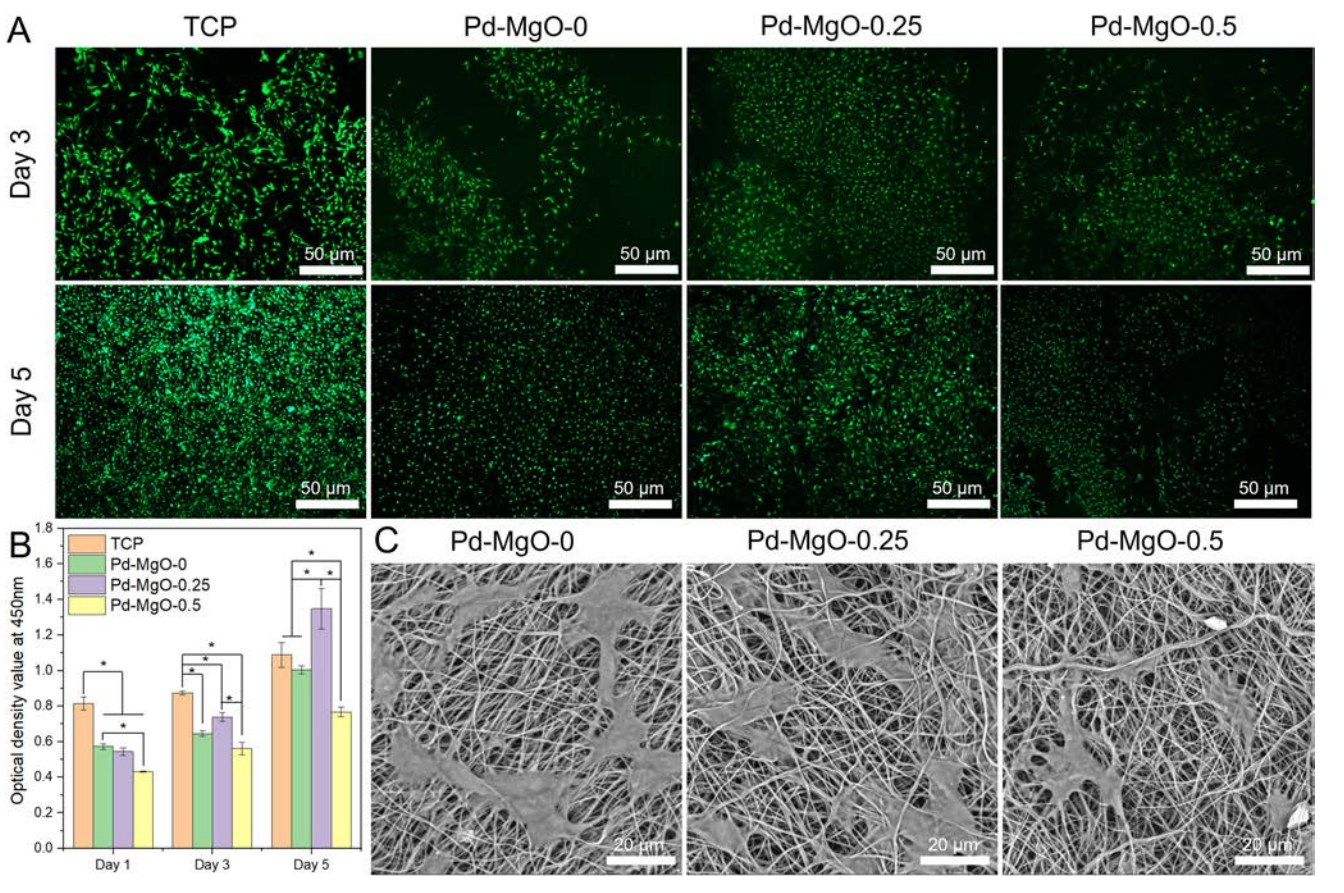

Fig. 4 NIH-3T3 cells cultured on TCP and various gingival nanofiber membranes. (A) Live/dead fluorescence staining merge images (green for live cells and red for dead cells) on days 3 and 5 of culture. (B) CCK-8 assay results on days 1, 3, and 5 of culture. (C) SEM images of NIH-3T3 cells on different gingival nanofiber membranes after 5 days of culture.

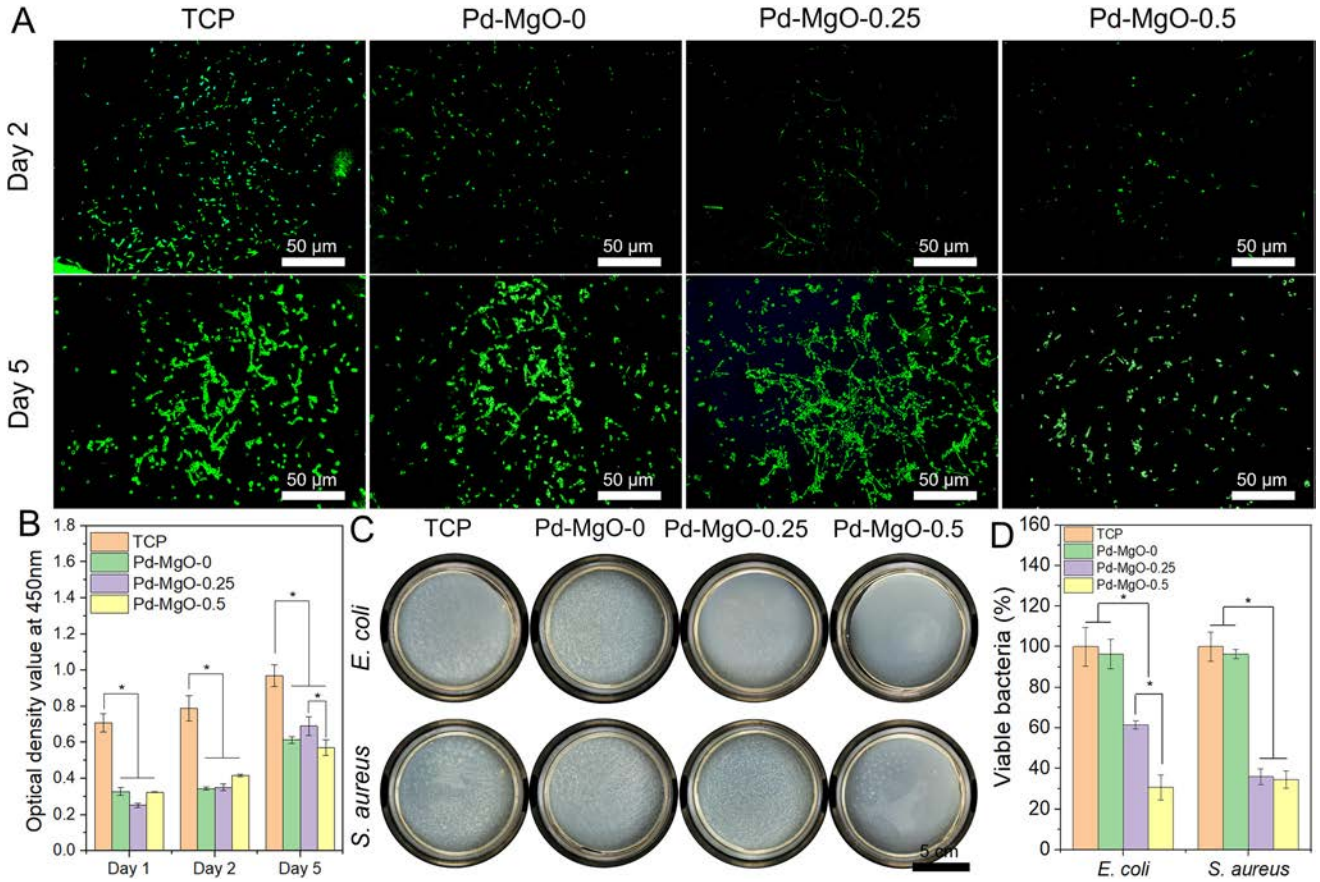

Fig. 5 RGF cells cultured on TCP and various gingival nanofiber membranes. (A) Live/dead fluorescence staining merged images (green for live cells and red for dead cells) on days 2 and 5 of culture. (B) CCK-8 assay results on days 1, 2, and 5 of culture. (C) Digital image of agar plates showing colony forming units of *E. coli* and *S. aureus* treated with TCP and gingival nanofibrous membranes. (D) Quantitative bacterial survival rates calculated from the corresponding colony forming units.

materials. Antibacterial tests (Fig. 5C) revealed that MgO-containing membranes exhibited significant antibacterial effects, with higher MgO content correlating with enhanced efficacy, suggesting that MgO's positive charge effectively disrupts bacterial membranes. The live/dead staining and CCK-8 assay results from Fig. 5A and B showed similar proliferation trends to those for NIH-3T3, with Pd–MgO-0.25 showing the highest effectiveness. However, proliferation on all membranes was lower than on TCP, indicating a preference for stiffer materials.[32,33]

Antimicrobial activity is extremely important for gingival membrane applications, and in this study, MgO was loaded on nanofiber membranes in order to achieve antimicrobial function. The antimicrobial effect of the nanofiber membrane and TCP on two common Gram-negative and Gram-positive bacteria, *E. coli* and *S. aureus*, is demonstrated in Fig. 5C and D. The results show that neither the nanofiber gingival membrane (Pd–MgO-0) nor TCP unloaded with MgO possesses an antibacterial effect. The antibacterial effect of the nanofiber gingival membrane with added MgO was significant, and this antibacterial effect was even more pronounced for *E. coli* bacteria as the amount of MgO increased. A large number of researchers have affirmed the antimicrobial effect of magnesium oxide and have attempted to theorize about it.[34,35] In the present study, we are more of the opinion that it is the release of magnesium ions that alters the pH in the environment, which in turn has a killing effect on bacterial survival.

3.3 Animal experiments and histological immunological evaluation of MgO-loaded nanofibrous membranes

To assess the gingival repair efficacy of the nanofibrous membranes, we established a soft tissue defect model in the rat maxilla. Control groups included untreated defects (Control) and commercial gelatin membranes (Commercial), alongside experimental groups with MgO-loaded (Pd–MgO-0.25) and non-MgO-loaded (Pd–MgO-0) membranes. The rat defects measured 2 mm × 0.5 mm; the Control group was untreated while others received the respective membranes, with samples harvested at ten days post-surgery (Fig. 6A and B). Histological analysis following HE and Masson staining indicated varying degrees of wound healing across groups, with epithelial layers largely restored. Unlike prior studies reporting visible defects at 3–7 days post-surgery due to a larger defect width, our ten-day evaluation demonstrated superior healing.[36] Nevertheless, differences in tissue repair emerged among the groups. The

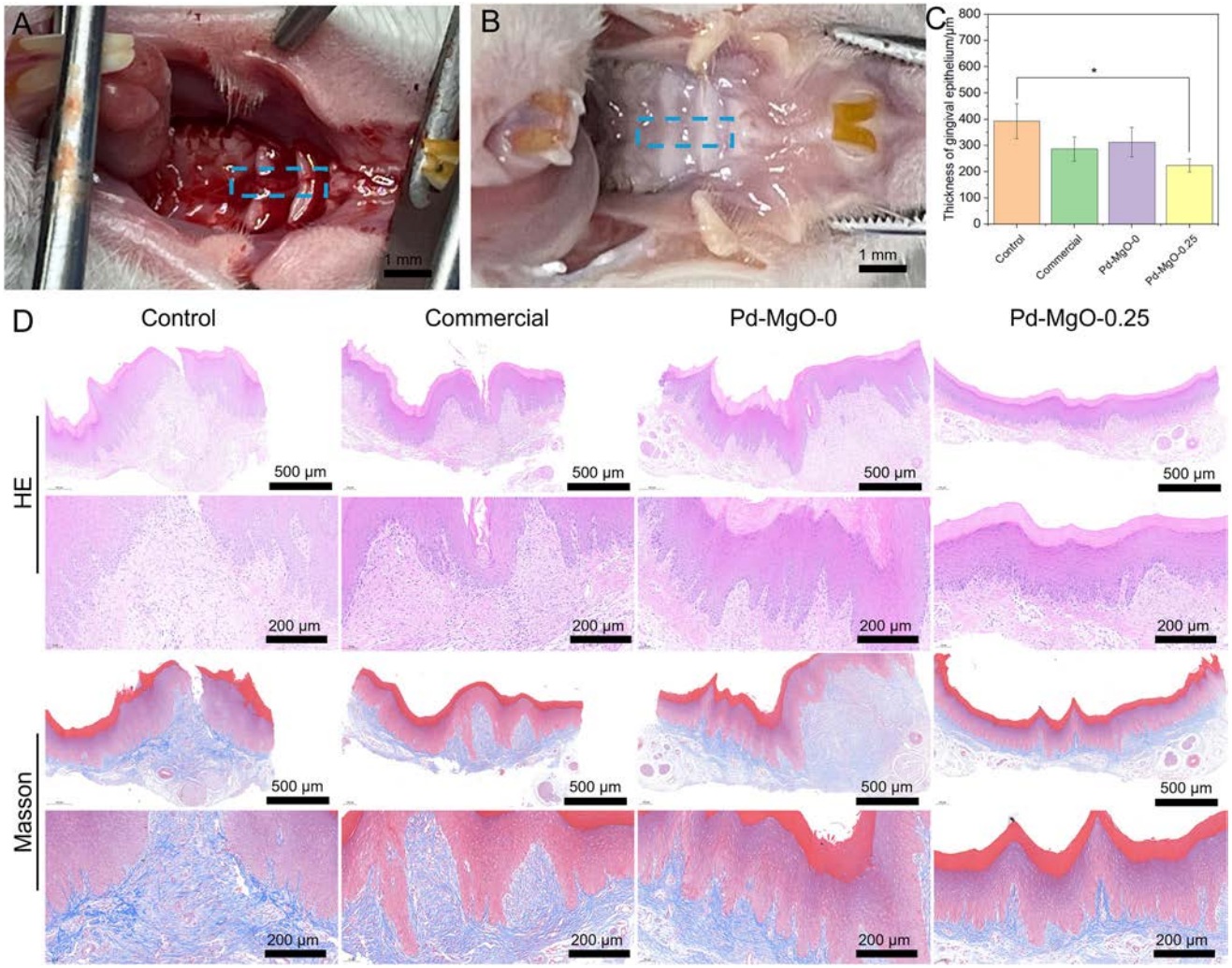

Fig. 6 (A) Intraoperative and (B) postoperative digital images of a rat gingival membrane defect model. (C) Statistical analysis of the regenerated gingival membrane's epithelial thickness post-surgery. (D) HE and Masson histological images of postoperative gingival tissue.

Control and Commercial groups exhibited disorganized collagen structures, indicating connective tissue proliferation, particularly in the Control group. In contrast, the Pd–MgO-0.25 group showed smoother, well-organized tissue with minimal overgrowth and a more mature epithelial layer (Fig. 6C). Statistical analysis revealed that the Pd–MgO-0.25 group had the thinnest epithelial layer, significantly lower than that in the Control group, suggesting that appropriate MgO levels promote efficient healing (Fig. 6D) potentially by supporting gingival fibroblast proliferation and inhibiting excessive scar formation.

Immunohistochemical analyses (Col-I, VEGF, IL-6, and TNF-α) were utilized to further evaluate maxillary soft tissue repair and inflammation. Fig. 6A shows the immunohistochemical results for Col-I and VEGF. Statistical analysis of positive areas indicated that the Commercial group had the highest Col-I expression, aligning with the Masson staining results, reflecting extensive collagen deposition and tissue proliferation. However, the Commercial group exhibited limited angiogenesis, possibly due to excessive collagen deposition leading to vascular regression. The Pd–MgO-0.25 group showed reduced angiogenesis compared to the Pd–MgO-0 group, likely due to Mg ions promoting tissue maturation. Further analysis of IL-6 and TNF-α expression (Fig. 7) showed that the Control group had elevated levels, indicating severe inflammatory responses, potentially impacting the healing outcomes. In contrast, the Commercial group presented the weakest inflammatory response, possibly due to the rapid degradation of gelatin with minimal foreign body reaction. The Pd–MgO-0 group displayed moderate inflammation, while the addition of Mg ions significantly reduced IL-6 and TNF-α levels, suggesting that Mg ions greatly mitigate inflammatory responses (Fig. 8).

In response to the clinical challenges of secondary trauma and donor site limitations associated with autogenous tissue transplantation for gingival defect repair, this study innovatively developed a magnesium oxide (MgO)-loaded nanofibrous gingival membrane. Compared to traditional collagen mem-

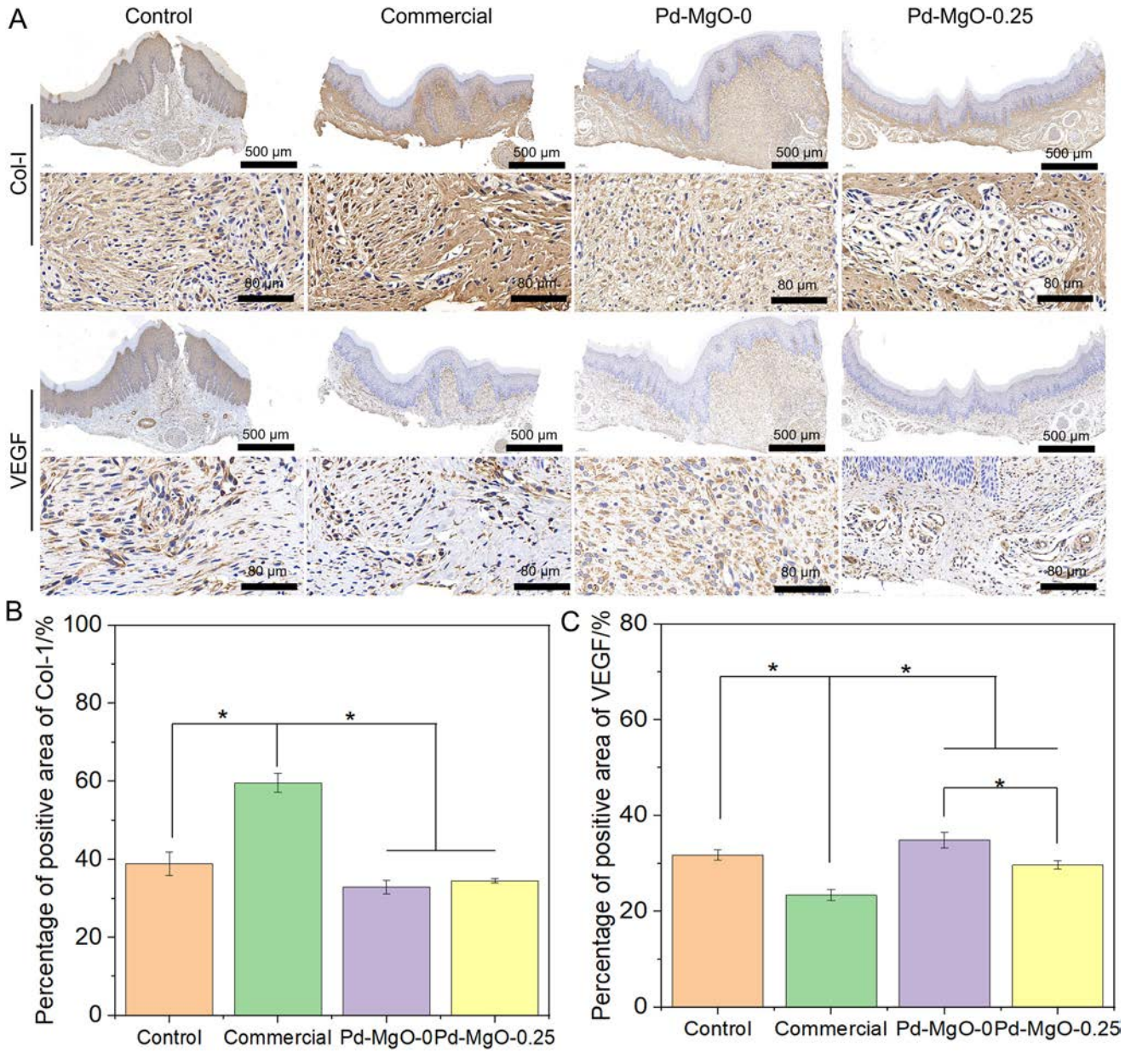

Fig. 7 (A) Immunohistochemical staining of Col-I and VEGF in the regenerative tissue of different groups. Relative positive area percentages of (B) Col-I and (C) VEGF.

branes (*e.g.*, Bio-Gide®), the PLGA/MgO composite membrane fabricated in this work demonstrates superior mechanical properties, with tensile strength being increased. Moreover, the sustained release of MgO confers dual biological effects. On the one hand, the presence of magnesium oxide (MgO) effectively inhibits bacterial growth, demonstrating significantly enhanced antibacterial properties compared to pure electrospun membranes. On the other hand, magnesium ions markedly promote fibroblast migration, while exhibiting favorable cytocompatibility at a content of 0.25 wt%. Animal experiments confirmed that this material effectively facilitates the repair of gingival defects in rats, with immunohistochemical analysis revealing a reduced inflammatory response. Notably, compared to reported silver-loaded nanomembranes, our material exhibits superior biosafety while maintaining antimicrobial efficacy. However, although the current study established a comprehensive system spanning material preparation to *in vitro* and *in vivo* evaluations, follow-up experiments incorporating large-animal mandibular models are required to address the complex biomechanical environment of maxillofacial regions, thereby strengthening the clinical translation evidence chain. Furthermore, understanding the significance of MgO and its metabolic pathways *in vivo* is critical, necessitating further molecular-level safety assessments.

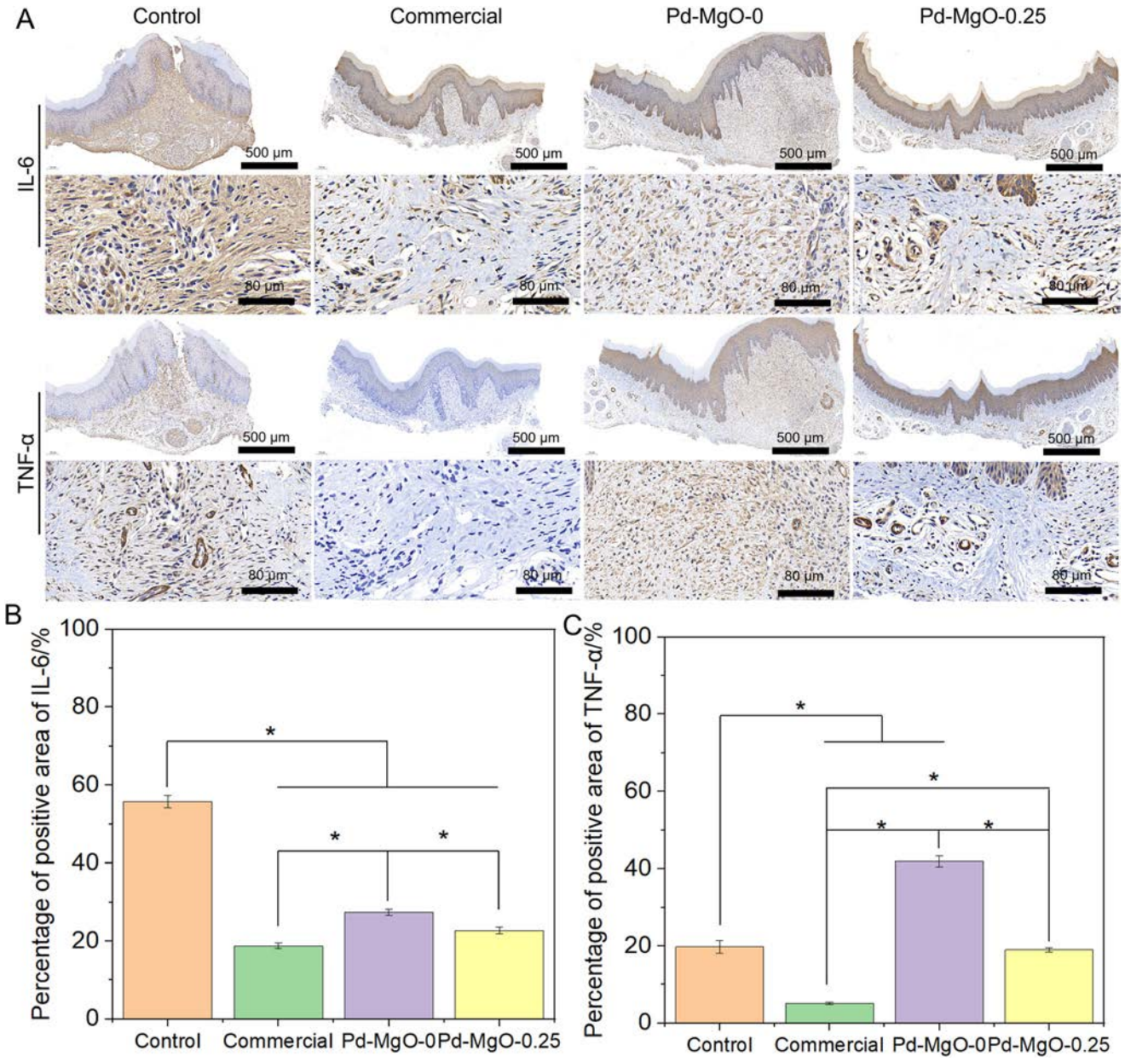

Fig. 8 (A) Immunohistochemical staining of IL-6 and TNF-α in the regenerative tissue of different groups. Relative positive area percentages of (B) IL-6 and (C) TNF-α.

4 Conclusion

The study concludes that PLA/dECM nanofibrous membranes loaded with MgO nanoparticles demonstrate potential for gingival tissue regeneration due to their antibacterial and anti-inflammatory properties. The optimal MgO concentration promoted cell proliferation, reduced inflammation, and supported gingival fibroblast function. The *in vivo* results in a rat model indicated efficient tissue regeneration, making this a promising approach for future applications in periodontal repair. However, further research is needed to confirm these findings in larger animal models and to investigate the long-term effects of MgO *in vivo*.

Author contributions

Shu Sun, Jing Qin, and Yifu Zhuang: conceptualization, methodology, and writing (original draft). Pengfei Cai and Xiao Yu: methodology, validation, and visualization. Hongsheng Wang, Xiumei Mo, and Jinglei Wu: conceptualization and supervision. Mohamed EL-Newehy and Meera Moydeen

Abdulhameed: resources and writing (review & editing). Mingyue Fan, Wenhao Qian, and Binbin Sun: conceptualization, funding acquisition, resources, and writing (review & editing).

Data availability

The data supporting the study are included in the main article. Any additional and raw data that were used during the preparation of the manuscript are available from the corresponding author upon request. The figure preparation includes professional tools like Adobe Photoshop, Origin, and Microsoft PowerPoint. Bibliographic references were prepared using the citing software Endnote.

For further inquiries or access to the data, please contact binbin.sun@dhu.edu.cn.

Conflicts of interest

There are no conflicts to declare.

Acknowledgements

This work was supported by the Fundamental Research Funds for the Central Universities (2232023D-10). This project was supported by the Medicine-Engineering Interdisciplinary Project of Shanghai Xuhui District Dental Center (SHXYFYG202306). This project was also supported by Researchers Supporting Project number (RSP2025R65), King Saud University, Riyadh, Saudi Arabia.

References

1 C. Vaquette, S. P. Pilipchuk, P. M. Bartold, D. W. Hutmacher, W. V. Giannobile and S. Ivanovski, *Adv. Healthcare Mater.*, 2018, **7**, 1800457.
2 R. J. Staples, S. Ivanovski and C. Vaquette, *J. Periodontal Res.*, 2020, **55**, 331–341.
3 A. Daghrery, J. A. Ferreira, J. Xu, N. Golafshan, D. Kaigler, S. B. Bhaduri, J. Malda, M. Castilho and M. C. Bottino, *Bioact. Mater.*, 2023, **19**, 268–281.
4 G. P. Prato, C. Clauser and P. Cortellini, *Periodontol. 2000*, 1995, **9**, 90–105.
5 E. G. Deliverska-Aleksandrova and D. K. Emilov, Effectiveness of Mucogingival Surgery for the Treatment of Gingival Recessions and Root Hypersensitivity, in *Advances in Gingival Diseases and Conditions*, ed. I.-G. Sufaru and S. M. Solomon, IntechOpen, Rijeka, 2024, DOI: **10.5772/intechopen.115147**.
6 S. Cao, Y. Zhao, Y. Hu, L. Zou and J. Chen, *Composites, Part B*, 2020, **202**, 108445.
7 H. Shokrani, A. Shokrani, M. Jouyandeh, F. Seidi, F. Gholami, S. Kar, M. T. Munir, D. Kowalkowska-Zedler, P. Zarrintaj and N. Rabiee, *ACS Appl. Bio Mater.*, 2022, **5**, 2107–2121.
8 M. Z. A. Zulkifli, D. Nordin, N. Shaari and S. K. Kamarudin, *Polymers*, 2023, **15**, 2418.
9 X. Xu, S. Ren, L. Li, Y. Zhou, W. Peng and Y. Xu, *J. Biomater. Appl.*, 2021, **36**, 55–75.
10 S. Wilk and A. Benko, *J. Funct. Biomater.*, 2021, **12**, 26.
11 E. Canciani, N. Gagliano, F. Paino, E. Amler, R. Divin, L. Denti, D. Henin, A. Fiorati and C. Dellavia, *Front. Mater.*, 2021, **8**, 670010.
12 J. Beznoska, J. Uhlík, A. Kestlerová, M. Královič, R. Divín, J. Fedačko, J. Beneš, M. Beneš, K. Vocetková, V. Sovková, A. Nečas, A. Nečasová, J. Holešovský and E. Amler, *Physiol. Res.*, 2019, **68**, S501–S508.
13 M. Lorencini, J. A. F. Silva, C. A. Almeida, A. Bruni-Cardoso, H. F. Carvalho and D. R. Stach-Machado, *Tissue Cell*, 2009, **41**, 43–50.
14 P. M. Bartold, *Aust. Dent. J.*, 1991, **36**, 255–268.
15 G. Dahlen, A. Basic and J. Bylund, *J. Clin. Med.*, 2019, **8**, 1339.
16 D. Celik and A. Kantarci, *Pathogens*, 2021, **10**, 1280.
17 L. Vitkov, J. Singh, C. Schauer, B. Minnich, J. Krunić, H. Oberthaler, S. Gamsjaeger, M. Herrmann, J. Knopf and M. Hannig, *Int. J. Mol. Sci.*, 2023, **24**, 4544.
18 P. Bhattacharya, A. Dey and S. Neogi, *J. Mater. Chem. B*, 2021, **9**, 5329–5339.
19 A.-P. Rodríguez-Hernández, A. L. Vega-Jiménez, A. R. Vázquez-Olmos, M. Ortega-Maldonado and L.-A. Ximenez-Fyvie, *Nanomaterials*, 2023, **13**, 502.
20 X. Liu, X. He, D. Jin, S. Wu, H. Wang, M. Yin, A. Aldalbahi, M. El-Newehy, X. Mo and J. Wu, *Acta Biomater.*, 2020, **108**, 207–222.
21 M. T. Wolf, K. A. Daly, E. P. Brennan-Pierce, S. A. Johnson, C. A. Carruthers, A. D'Amore, S. P. Nagarkar, S. S. Velankar and S. F. Badylak, *Biomaterials*, 2012, **33**, 7028–7038.
22 Y. Fang, Y. Han, S. Wang, J. Chen, K. Dai, Y. Xiong and B. Sun, *Biomater. Adv.*, 2022, **138**, 212951.
23 X. Wen, J. Xiong, S. Lei, L. Wang and X. Qin, *Adv. Fiber Mater.*, 2021, 1–17.
24 Y. J. Shin, R. T. Shafranek, J. H. Tsui, J. Walcott, A. Nelson and D.-H. Kim, *Acta Biomater.*, 2021, **119**, 75–88.
25 D. Chen and W. Zhen, *Polym. Test.*, 2021, **100**, 107232.
26 N. F. Mazuki, Y. Nagao, M. Z. Kufian and A. S. Samsudin, *Mater. Today: Proc.*, 2022, **49**, 3105–3111.
27 S. Sagadevan, S. Venilla, A. R. Marlinda, M. Johan, Y. A. Wahab, R. Zakaria, A. Umar, H. H. Hegazy, H. Algarni and N. Ahmad, *J. Nanosci. Nanotechnol.*, 2020, **20**, 2488–2494.
28 Z. Hussain, P. Ding, L. Zhang, Y. Zhang, S. Ullah, Y. Liu, I. Ullah, Z. Wang, P. Zheng and R. Pei, *Biomed. Mater.*, 2022, **17**, 034102.
29 J. Ravoor, S. Amirthalingam, T. Mohan and J. Rangasamy, *Colloid Interface Sci. Commun.*, 2020, **39**, 100332.
30 H. Qin, J. Weng, B. Zhou, W. Zhang, G. Li, Y. Chen, T. Qi, Y. Zhu, F. Yu and H. Zeng, *Biol. Trace Elem. Res.*, 2023, **201**, 2823–2842.

31 C. Leibiger, N. Kosyakova, H. Mkrtchyan, M. Glei, V. Trifonov and T. Liehr, *J. Histochem. Cytochem.*, 2013, **61**, 306–312.
32 Y. Wang, G. Wang, X. Luo, J. Qiu and C. Tang, *Burns*, 2012, **38**, 414–420.
33 J. Zhong, Y. Yang, L. Liao and C. Zhang, *Biomater. Sci.*, 2020, **8**, 2734–2755.
34 N.-Y. T. Nguyen, N. Grelling, C. L. Wetteland, R. Rosario and H. Liu, *Sci. Rep.*, 2018, **8**, 16260.
35 Y. He, S. Ingudam, S. Reed, A. Gehring, T. P. Strobaugh and P. Irwin, *J. Nanobiotechnol.*, 2016, **14**, 1–9.
36 F. Chen, X. Liu, X. Ge, Y. Wang, Z. Zhao, X. Zhang, G.-Q. Chen and Y. Sun, *Chem. Eng. J.*, 2023, **451**, 138899.